Science AAAS

Incision into the Eastern Andean Plateau During Pliocene Cooling

Richard O. Lease and Todd A. Ehlers

Science **341**, 774 (2013);
DOI: 10.1126/science.1239132

Incision into the Eastern Andean Plateau During Pliocene Cooling

Richard O. Lease*† and Todd A. Ehlers

Canyon incision into mountain topography is commonly used as a proxy for surface uplift driven by tectonic or geodynamic processes, but climatic changes can also instigate incision. The ~1250-kilometer (km)–long eastern margin of the Andean Plateau hosts a series of 1.5- to 2.5-km-deep canyons that cross major deformation zones. Using (U-Th)/He thermochronology, we document a transition from Miocene faulting to Pliocene canyon incision across the northeastern plateau margin. Regionally, widespread Pliocene incision into the eastern plateau margin is concurrent with a shift in global climate from early Pliocene warmth to late Pliocene cooling. Enhanced moisture transport onto the Andean Plateau driven by sea surface temperature changes during cooling is the likely pacemaker for canyon incision.

Defining the role of tectonic and climate processes in shaping mountain topography is often limited by an inability to discern among different exhumation mechanisms. Deep canyons have been carved into high-elevation, low-relief terrain along both flanks of the Andean Plateau (Fig. 1). Reconstructing the space-time pattern of incision across the plateau can illuminate the ultimate causes for incision. On the western plateau margin, the onset of canyon incision ~9 million years ago (Ma) (*1*, *2*) has been interpreted as a consequence of plateau-wide surface uplift driven by geodynamic processes (*3*), although this view has been challenged (*4*). A close look at the eastern plateau margin suggests that headward canyon incision into high-elevation terrain accelerated in the past few million years (My) (*5*, *6*).

The humid northeastern plateau margin is a well-constrained tectonic and geomorphic boundary where the timing of incision is unknown. The physiography and geology of the northeastern plateau margin reveals large magnitudes of both river incision and faulting in southern Peru (Fig. 2). In this area, deformation is concentrated along the Eastern Cordillera reverse fault zone (Fig. 2A), which thrusts Paleozoic over Triassic sediments with 5 to 7 km of vertical offset (*7*, *8*) (fig. S1). In addition, several canyons dissect the plateau margin in this region, incising into the low-relief plateau surface presently at elevations of >4 km (Fig. 2, B and C). Minimal net glacial erosion of the plateau is suggested by the preservation of 6 Ma volcanics (*9*) beneath the Quelccaya ice cap (*10*) and the lack of a systematic correlation between topography and glacier equilibrium line altitudes (*11*) (Fig. 2D). Locally, the Eastern Cordillera reverse fault is exposed at the midpoint of the 2.5-km-deep Rio San Gaban canyon (Fig. 2D).

We examined the cooling history of the upper crust in the Rio San Gaban canyon to determine when erosion accelerated in response to faulting versus incision. We used (U-Th)/He thermochronology for the minerals apatite (AHe) and zircon (ZHe), with effective closure temperatures (T_c) of ~60°C and ~180°C, respectively (*12*). We collected a single suite of samples within a dual reference frame: (i) on either side of a major crustal fault and (ii) within an incised canyon (Fig. 2D). Of 11 samples collected, 7 (5) yielded apatite (zircon) suitable for dating, primarily from Triassic and Jurassic plutons (tables S1 to S3). Our three lowest-elevation sample sites had been previously analyzed for biotite K/Ar thermochronology (BAr) (*13*), with a T_c of ~350°C (*12*).

ZHe ages exhibit a sharp discontinuity across the fault that reveals differential Miocene erosion (Fig. 3A). On the hanging-wall, samples from a 1560- to 2060-m range of elevations have identical 15 Ma ZHe cooling ages. This consistency suggests that rapid thrust-induced rock uplift and erosion of the hanging-wall was ongoing by middle Miocene time, with 4 to 6.4 km of exhumation since then (assuming a geothermal gradient range of 25° to 40°C/km). In contrast, samples on the footwall have a wider 76- to 94-Ma range of ZHe ages that define a period of older, slower cooling. Overall, this pattern indicates that rapid Miocene erosion was limited to the hanging-wall, with fault-related deformation imposing a fundamental control.

Pronounced differential erosion across the fault is also evident with higher temperature chronometers. On the hanging-wall, BAr ages (*13*) increase linearly from 87 to 125 Ma with increasing elevation and indicate slow cooling within a partial retention zone (Fig. 3A). These late Cretaceous BAr ages (T_c = 350°C) on the hanging-wall are now juxtaposed against a wide range of late Cretaceous ZHe ages (T_c = 180°C) on the footwall. Thermal histories derived from inverse modeling of thermochronometer ages (*14*) corroborate disparate late Cretaceous-Miocene cooling for hanging-wall versus footwall samples (Fig. 3C). The ~150°C difference in cooling/erosion magnitude across the fault demonstrates large reverse fault displacement that initiated at or before ~20 Ma.

In contrast to discontinuous ZHe and BAr ages, AHe ages are identical on either side of the fault and suggest that Pliocene erosion was independent of deformation patterns (Fig. 3, A and B). Samples from a wide 1700-m range of elevation within an incised canyon have a narrow 4.1- to 2.8-Ma range of AHe ages, reflecting rapid, synchronous erosion of both hanging-wall and footwall blocks by this time. Modeled thermal histories of individual sam-

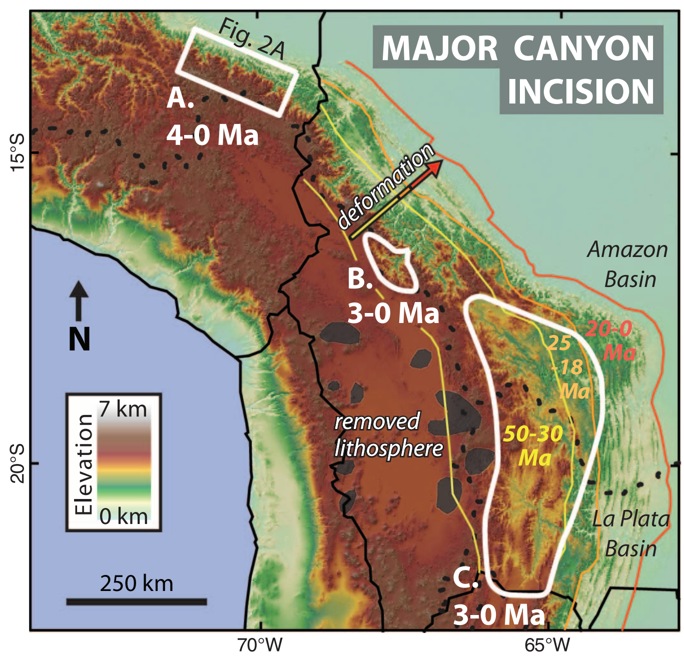

Fig. 1. Pliocene canyon incision into the eastern margin of the Andean Plateau. Study areas for (**A**) Rio San Gaban, (**B**) Rio La Paz (*6*, *16*), and (**C**) San Juan del Oro (*5*). Eastern Andes deformation fronts and timing are denoted by colored lines: yellow, Eastern Cordillera; orange, Interandean; red, Subandean (*16*–*18*). Removed mantle lithosphere is denoted by black polygons (*19*). Amazon and La Plata watersheds are outlined with black dashed line.

Department of Geosciences, University of Tübingen, Tübingen 72074, Germany.

*Present address: U.S. Geological Survey, Anchorage, AK 99508, USA.

†Corresponding author. E-mail: rlease@usgs.gov

ples corroborate this finding of rapid Pliocene erosion (Fig. 3C), and we estimate at least 1 to 1.6 km of exhumation for each sample (geothermal gradient range of 25° to 40°C/km). The low-relief plateau surface capping the canyon, on the other hand, displays only minor Pliocene exhumation: One footwall sample exhibits scattered single-grain ages suggestive of slow Miocene-Pliocene cooling, which is consistent with minimal erosion of the 6 Ma volcanic deposits upstream. Beneath the low-relief plateau surface, 4- to 3-Ma cooling ages present at incision depths of 1.9 to 2.4 km in the canyon suggest that rapid incision of the modern canyon began in Pliocene time without displacement on the fault (Fig. 3B). Although AHe ages do not correlate with distance along the transect, we estimate a vertical incision rate of 0.6 km/My and a headward incision rate ≥ 9 km/My since 4 Ma, which are comparable to rates estimated for the northwestern margin of the Andean Plateau (*15*). We interpret Pliocene erosion to reflect a fundamental shift, when rivers began incising rapidly into the northeastern plateau margin and across an inactive major fault (fig. S2).

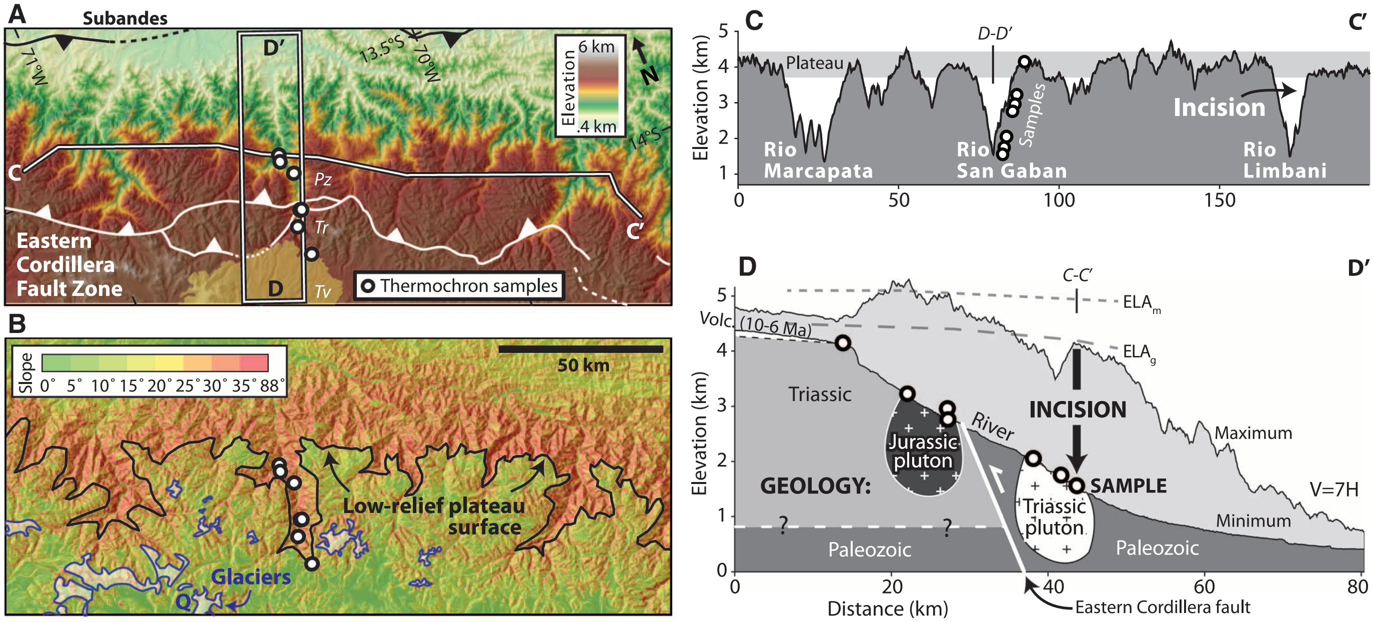

Fig. 2. Tectonic and geomorphic setting of canyons on the northeastern Andean Plateau margin. (**A**) Tectonic context: topography and major geology. Tertiary deformation was concentrated along the Eastern Cordillera reverse fault zone (5 to 7 km of vertical offset) (*7*). Tv, Tertiary volcanics (*9*); Tr, Triassic Mitu Group; Pz, Paleozoic sedimentary rocks. (**B**) Geomorphic context: Slope map showing extent of low-relief plateau surface, modern glaciers, and high-relief plateau margin. Threshold hillslopes adjacent to incised canyons erode primarily by landsliding. Q, Quelccaya ice cap (*10*). (**C**) Topographic profile C-C′ (parallel to plateau margin) showing 2.5-km-deep canyons incised into low-relief plateau surface at elevations >4 km. Sample locations projected onto profile. (**D**) Swath topographic profile D-D′ (perpendicular to plateau margin) showing structural and geomorphic context of thermochronology sampling transect. ELA, glacier equilibrium line altitude: m, modern; g, glacial (*11*).

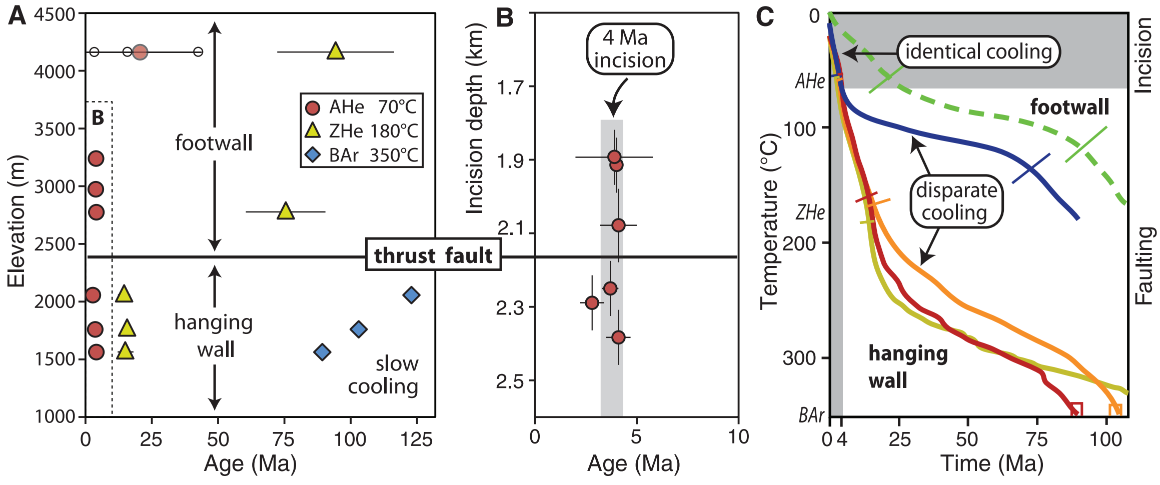

Fig. 3. Thermochronological results from the San Gaban Canyon, northeastern Andean Plateau margin. (**A**) Cooling ages versus elevation. AHe, apatite (U-Th)/He; ZHe, zircon (U-Th)/He; and BAr, biotite K/Ar. He age error at ± 2σ standard error. (**B**) AHe cooling ages versus incision depth. Age error at ± 2σ standard error. Incision depth = maximum swath elevation – sample elevation (see Fig. 2D). (**C**) Thermal histories of individual samples with paired AHe-ZHe (-BAr) cooling ages. Lines are weighted mean cooling paths from inverse modeling (*14*). Colored error bars delimit extent of all "good" model fits in the vicinity of thermochronometer analyses and are drawn orthogonal to the cooling path. Weighted mean cooling paths predict observed ages either exactly or within 0.3 My. Range of model solutions reported in fig. S3.

Pliocene incision into the eastern margin of the Andean Plateau is widespread (Fig. 1). Volcanic chronostratigraphy from basins on the plateau margin indicate deposition until ~3 Ma and incision thereafter. On the southeastern margin, major incision of 1-km-deep canyons into the extensive San Juan del Oro erosion surface did not occur until after ~3 Ma, several million years after the erosion surface formed between 12 and 9 Ma (*5*). Similar in timing, breaching of the central portion of the internally drained Altiplano basin occurred since ~3 Ma via incision of the Rio La Paz through the Eastern Cordillera (*6*, *16*). On the northeastern plateau margin, our results indicate the onset of bedrock cooling due to rapid canyon incision by 4 to 3 Ma (Fig. 3). Over >1250-km distances, regional incision into the eastern margin of the Andean Plateau has accelerated since 4 to 3 Ma (*5*, *6*, *16*) (Figs. 1 and 3).

Pliocene incision into the eastern Andean Plateau occurred across different tectonic, geodynamic, and catchment boundaries, suggesting that a mechanism unrelated to these fields was responsible for incision. Several examples support this. First, the >1250 km along-strike extent of Pliocene incision crosses areas with wide-ranging deformation histories (20 to 50 Ma) and exhumation magnitudes (4 to 10 km) (*17*) that suggest that Pliocene incision was decoupled from active deformation (Fig. 1). Furthermore, movement on basement megathrust faults that could drive hinterland surface uplift above crustal ramps had ceased by 20 to 25 Ma (*16*, *18*) in the incised areas. To the east of our canyon transect, limited deformation in the Subandes has occurred since 15 Ma [<30% shortening (*8*)], suggesting that crustal thickening and isostatic compensation alone did not drive surface uplift and erosion in the past 4 My. Second, geodynamic mechanisms are limited to small areas and are thus unable to drive regional surface uplift and rapid Pliocene incision over >1250 km. For example, piecemeal removal of lithospheric mantle has only been documented for isolated areas <150 km wide (Fig. 1) (*19*). Likewise, other geodynamic mechanisms such as lower crustal flow, flat slab subduction, or an increase in the taper angle of the fold and thrust belt are geographically limited and/or incremental processes. Third, drainage capture is unable to drive the 1.5- to 2.5-km-deep incision observed because incised catchments persistently graded to near sea level close to the mountain front (*20*), and the catchments span a broad area in both the Amazon and La Plata watersheds. Thus, the lack of a correlation between regional incision and localized tectonic, geodynamic, or drainage reorganization phenomena suggests that a regional mechanism such as climate change triggered incision and that surface uplift and canyon incision are temporally decoupled.

Large magnitudes of climate change were coeval with the Pliocene onset of rapid river incision documented here. Tropical precipitation patterns were fundamentally affected by sea surface temperature (SST) changes during the global transition from early Pliocene warmth to late Pliocene cooling (*21*). First, the late Pliocene strengthening of both zonal and meridional SST gradients in the equatorial Pacific, together with shoaling of the thermocline (*21*), heralds the transition from early Pliocene "permanent" El Niño–like conditions to the late Pliocene onset of the El Niño–Southern Oscillation (ENSO) (*22*). Altiplano precipitation on interannual time scales is particularly sensitive to ENSO phase. A precipitation increase occurs during La Niña when upper-level easterlies transport convective Amazon rainfall onto the plateau (*23*), whereas a precipitation decrease occurs during El Niño when westerlies dominate. Second, the late Pliocene marks the onset of protracted north Atlantic cooling (*21*, *24*). Amazon moisture flux is enhanced (*25*) when a strengthened Atlantic meridional SST gradient displaces the Intertropical Convergence Zone southward (*26*). Intensified Altiplano precipitation on millennial time scales is linked to North Atlantic cold events (*27*). In contrast to orographic rainfall established at lower elevations along the eastern Cordillera since 15 to 11 Ma (*17*, *28*), moisture flux into the high elevation Altiplano was not favored until Pacific and Atlantic SST gradients changed at 4 to 3 Ma (*21*).

We propose that enhanced moisture flux into the Altiplano drove rapid incision (*29*) of its eastern margin starting at 4 to 3 Ma (Fig. 1). During modern La Niña, a fourfold increase in heavy storm events and twofold increase in specific stream power drives both vigorous Andean incision (*30*) upstream and episodic sedimentation in the Amazon (*31*) downstream. Furthermore, Quaternary glacier growth and lake expansion on the Altiplano were driven both by periods of La Niña–like conditions (*10*, *32*, *33*) and periods of Northern Hemisphere cooling (*25*, *27*, *34*, *35*), with up to threefold increases in precipitation (*36*). On million-year time scales, the 4- to 3-Ma onset of eastern Andean Plateau dissection (Fig. 1), glaciation (*37*), and plateau lakes (*38*) suggest that enhanced Altiplano precipitation began in the late Pliocene. Given this consistency and the lack of plausible tectonic drivers for incision, we conclude that SST-driven precipitation changes during global cooling regulated late Pliocene incision into the eastern Andean Plateau.

References and Notes

1. T. F. Schildgen, K. V. Hodges, K. X. Whipple, P. W. Reiners, M. S. Pringle, *Geology* **35**, 523–526 (2007).
2. G. D. Hoke *et al*., *Tectonics* **26**, TC5021 (2007).
3. C. N. Garzione *et al*., *Science* **320**, 1304–1307 (2008).
4. T. A. Ehlers, C. J. Poulsen, *Earth Planet. Sci. Lett.* **281**, 238–248 (2009).
5. L. Kennan, S. H. Lamb, L. Hoke, *Geol. Soc. London Spec. Publ.* **120**, 307–323 (1997).
6. G. Zeilinger, F. Schlunegger, *Terra Nova* **19**, 373–380 (2007).
7. V. Carlotto, *Bol. Soc. Geol. Peru* **101**, 91–119 (2006).
8. N. Gotberg, N. McQuarrie, V. C. Caillaux, *Geol. Soc. Am. Bull.* **122**, 727–742 (2010).
9. A. Cheilletz *et al*., *Tectonophysics* **205**, 307–327 (1992).
10. L. G. Thompson, E. Mosley-Thompson, B. M. Arnao, *Science* **226**, 50–53 (1984).
11. A. G. Klein, G. O. Seltzer, B. L. Isacks, *Quat. Sci. Rev.* **18**, 63–84 (1999).
12. P. W. Reiners, M. T. Brandon, *Annu. Rev. Earth Planet. Sci.* **34**, 419–466 (2006).
13. D. J. Kontak, E. Farrar, A. H. Clark, D. A. Archibald, *J. S. Am. Earth Sci.* **3**, 231–246 (1990).
14. R. A. Ketcham, *Rev. Mineral.* **58**, 275–314 (2005).
15. T. F. Schildgen, G. Balco, D. L. Shuster, *Earth Planet. Sci. Lett.* **293**, 377–387 (2010).
16. N. McQuarrie, J. B. Barnes, T. A. Ehlers, *Tectonics* **27**, TC3007 (2008).
17. J. B. Barnes, T. A. Ehlers, N. Insel, N. McQuarrie, C. J. Poulsen, *Geology* **40**, 1135–1138 (2012).
18. B. K. Horton, *Tectonics* **24**, TC3011 (2005).
19. S. L. Beck, G. Zandt, *J. Geophys. Res.* **107**, 2230 (2002).
20. C. Hoorn *et al*., *Science* **330**, 927–931 (2010).
21. A. V. Fedorov *et al*., *Nature* **496**, 43–49 (2013).
22. A. V. Fedorov *et al*., *Science* **312**, 1485–1489 (2006).
23. R. Garreaud, M. Vuille, A. C. Clement, *Palaeogeogr. Palaeoclimatol. Palaeoecol.* **194**, 5–22 (2003).
24. M. Mudelsee, M. E. Raymo, *Paleoceanography* **20**, PA4022 (2005).
25. L. G. Thompson *et al*., *Science* **340**, 945–950 (2013).
26. J. C. Chiang, M. Biasutti, D. S. Battisti, *Paleoceanography* **18**, 1094 (2003).
27. P. A. Baker *et al*., *Science* **291**, 640–643 (2001).
28. C. J. Poulsen, T. A. Ehlers, N. Insel, *Science* **328**, 490–493 (2010).
29. K. L. Ferrier, K. L. Huppert, J. T. Perron, *Nature* **496**, 206–209 (2013).
30. B. Bookhagen, M. R. Strecker, in *Amazonia: Landscape and Species Evolution*, C. Hoorn, F. P. Wesselingh, Eds. (Wiley-Blackwell Publishing Ltd., Oxford, UK, 2010), pp. 223–241.
31. R. Aalto *et al*., *Nature* **425**, 493–497 (2003).
32. R. S. Bradley, M. Vuille, D. Hardy, L. G. Thompson, *Geophys. Res. Lett.* **30**, 1174 (2003).
33. C. J. Placzek, J. Quade, P. J. Patchett, *Geol. Soc. Am. Bull.* **118**, 515–532 (2006).
34. L. G. Thompson *et al*., *Science* **282**, 1858–1864 (1998).
35. S. C. Fritz *et al*., *Quat. Res.* **68**, 410–420 (2007).
36. C. J. Placzek, J. Quade, P. J. Patchett, *Earth Planet. Sci. Lett.* **363**, 97–108 (2013).
37. C. M. Clapperton, *Nature* **277**, 375–377 (1979).
38. R. Gaupp, A. Kött, G. Wörner, *Palaeogeogr. Palaeoclimatol. Palaeoecol.* **151**, 79–100 (1999).

Acknowledgments: We thank E. Enkelmann and P. Reiners for laboratory assistance, N. Eichelberger for field assistance, and the NSF Continental Dynamics program for support (EAR-0907817 to T.A.E.). The data reported in this paper are available in the supplementary materials.

Supplementary Materials

www.sciencemag.org/cgi/content/full/341/6147/774/DC1
Materials and Methods
Figs. S1 to S3
Tables S1 to S3
References (*39*–*42*)

15 April 2013; accepted 15 July 2013
10.1126/science.1239132